Inorganic Chemistry

Article

pubs.acs.org/IC

Replica of a Fishy Enzyme: Structure–Function Analogue of Trimethylamine-N-Oxide Reductase

Golam Moula,[†] Moumita Bose,[†] and Sabyasachi Sarkar*[,‡]

[†]Department of Chemistry, Indian Institute of Technology, Kanpur, Kanpur-208016, Uttar Pradesh, India

[‡]Department of Chemistry, Bengal Engineering and Science University, Shibpur, Botanic Garden, Howrah 711103, West Bengal, India

Supporting Information

ABSTRACT: Three new complexes, $[Mo^{IV}O(mnt)(SS)]^{2-}$ (SS = dimethylethylenedicarboxylate (DMED), toluenedithiolate (tdt), benzenedithiolate (bdt); mnt = maleonitriledithiolate), each possessing two different dithiolene ligands, are synthesized as model of trimethylamine-N-oxide reductase. The asymmetric dithiolene ligands present in these complexes simulate the two different (P and Q) pterin coordinations in the family of DMSO reductase. These complexes reduce trimethylamine-N-oxide ($(CH_3)_3N^+-O^-$ or TMANO), the biological substrate of trimethylamine-N-oxide reductase, to trimethylamine ($(CH_3)_3N$), responsible for the fishy smell of dead aquatic animals. The reaction kinetics of trimethylamine-N-oxide reduction by these complexes follow the Michaelis–Menten saturation kinetics. These experimental findings have been rationalized by DFT, TD-DFT level of calculations.

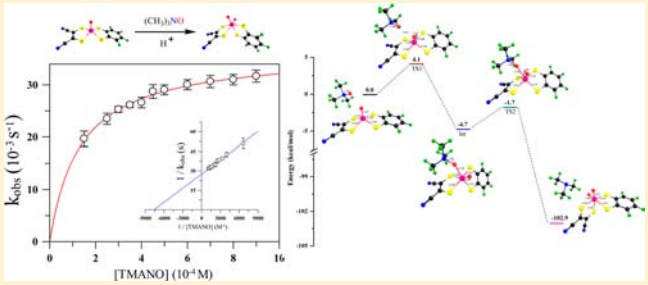

INTRODUCTION

Marine animals like fish under natural habitation produce $(CH_3)_3N^+-O^-$ (TMANO) as osmoprotector.[1] In dead fish the nonavailability of oxygen induces the enteric bacteria, *E. coli*, to change their respiration from aerobic to anaerobic under TMANO. The induced enzyme, trimethylamine N-oxide reductase (TMANOR),[1] of the *E. coli* now uses TMANO as the terminal electron acceptor instead of oxygen. Under such anaerobic respiration these bacteria release trimethylamine (eq 1) which has the dreadful smell of rotting fish.

$$\text{enzyme}-Mo^{IV} + (CH_3)_3N^+-O^- + 2H^+ \rightarrow \text{enzyme}-Mo^{VI} + (CH_3)_3N + H_2O \quad (1)$$

In human, a copper containing monoxygenase catalyzes the oxidation of the metabolite trimethylamine to odorless TMANO. The malfunction of this enzyme known as "fish odor syndrome" is a genetic disorder in human.[2] TMANOR belongs to the DMSO reductase (DMSOR) family.[3] The crystal structure of TMANOR from *Shewanella massilia* is reported at 2.5 Å resolution with an unusual seven-coordinate molybdenum,[4] and the active site structure remains anomalous. X-ray absorption spectroscopy showed that, like DMSOR,[5] the active site of TMANOR can exist in different forms.[6] However, in all these forms the common feature is the presence of two dithiolate coordinated dinucleotide variants of pyranopterin-dithiolate (molybdopterin (MPT)) ligands. The other important finding is the presence of desoxo Mo instead of terminal oxo group in the structurally characterized DMSOR. Interestingly, in the oxidase family of molybdoenzymes the presence of a terminal oxo as (Mo=O) moiety is unique in association with only one pyranopterin-dithiolate coordination. Thus, in sulfite oxidase a terminal oxo group is conserved in its enzymatic reaction and remained as spectator oxo ligand.[3] The presence of such (Mo=O) group is presumed to be essential to impart stability considering the coordination of only one pyranopterin-dithiolate to molybdenum. In contrast the reductase class of enzymes are stabilized by two dithiolate coordination and therefore may afford to utilize desoxo coordination.

Interestingly, DMSOR can utilize TMANO as an alternate substrate but TMANOR seldom utilizes DMSO as the alternate substrate[7a] (TMANO being a stronger oxo transfer agent compared to that of DMSO thus transfers oxygen both to TMANOR and DMSOR). There may be certain variation around the Mo center in the respective active site of these two proteins for the substrate specificity.[7b] The profound H-bonding interaction prevalent near the active site to stabilize the Mo-cofactor in these proteins[4] may have a certain role to interact with the zwitterions nature of TMANO.

There are several reports[8] to utilize the TMANO as a good oxo transfer reagent to synthesize dioxo Mo(VI) complex from the corresponding Mo(IV) monoxo species by simple oxo transfer reaction. However, the kinetics of such reaction has been widely varied. It has been argued that such oxidation reaction is promoted by NH···SH-bonding and the rate is faster when such H-bonding is intramolecular rather than inter-

Received: January 31, 2013
Published: April 17, 2013

   dx.doi.org/10.1021/ic4002576 | *Inorg. Chem.* 2013, 52, 5316–5327

molecular.[9] Later it was proposed that such reaction involved the cis attack of TMANO to the Mo center which is the rate determining step that is followed by the product formation and without any cis−trans rearrangement.[9] Recently, Sugimoto et al. reported the synthesis of dioxo Mo(VI) from monoxo Mo(IV) complex with two structurally different dithiolenes and the reaction that followed is second order kinetics.[10]

It is suggested that the two different pterin derivatives namely P and Q pterin in DMSOR family of enzymes modulate the redox potential of the active site. This facilitates the electron transfer with ready regeneration of the Mo^{IV} center which finally activates the active site for oxygen-atom transfer reaction.[11]

The variation in oxo-transfer kinetics observed in different synthesized complexes prompted us to revisit the kinetic aspect using some newly designed model complexes. In this work we used three complexes each with the coordination of two structurally different dithiolene ligands to proxy P and Q pterins. Among these we conserved mnt^{2-} as the common dithiolene ligand with the variation of other dithiolene ligand in each case. The mnt^{2-} was used as the nonvariant ligand as complexes containing mnt^{2-} ligand closely followed enzymatic reaction.[12]

EXPERIMENTAL SECTION

Materials. All reactions and manipulations were performed under ambient conditions. $(CH_3)_3N^+-O^-\cdot 0.2H_2O$, benzenedithiol, toluenedithiol, and dimethyl-acetylenedicarboxylate were obtained from Aldrich. Na_2MoO_4, acetic acid, and Et_4NBr were obtained from S. D. Fine Chemicals Ltd., India. Solvents were used as received. Na_2mnt ($mnt^{2-} = S_2C_2(CN)_2^{2-}$ = 1, 2-dicyanoethylenedithiolate) was prepared by the method of Stiefel et al.[13] Synthesis of $[Et_4N]_2[Mo^{IV}O(S_4)_2]$ (**1**) was modified following the procedures reported earlier.[14]

Physical Measurements. Elemental analyses for carbon, hydrogen, nitrogen, and sulfur were measured with Perkin-Elmer 2400 microanalyzer. Infrared spectra were recorded on a Bruker Vertex 70, FT-IR spectrophotometer as pressed KBr disks. Electronic spectra were recorded on Lambda 35 UV−vis spectrometer (Perkin−Elmer) with PCB 150/PTP-6 Peltier System. Cyclic voltammetric measurements were made with a BASi Epsilon-EC Bioanalytical Systems, Inc. instrument. Cyclic voltammograms of 10^{-3} M solution of the compounds were recorded with a glassy carbon electrode as working electrode, 0.2 M Bu_4NClO_4 as supporting electrolyte, Ag/AgCl electrode as reference electrode, and a platinum auxiliary electrode. All electrochemical experiments were done under argon atmosphere at 298 K. Potentials are referenced against internal ferrocene (Fc) and are reported relative to the Ag/AgCl electrode ($E_{1/2}(Fc^+/Fc)$) 0.459 V versus Ag/AgCl electrode.

Synthesis. $[Et_4N]_2[Mo^{IV}O(S_4)_2]$ (1). $[Et_4N]_2[Mo^{IV}O(S_4)_2]$ was synthesized by a modified procedure of the earlier method.[14] Rapid to moderate flow of H_2S was bubbled into a stirred solution of 10 g elemental sulfur in 25 mL of NH_3 for 30 min. A 15−17 mL portion of this solution was rapidly added via frit to a filtered solution of 5 g of $(NH_4)_6[Mo_7O_{24}]\cdot 4H_2O$ in 200−250 mL water with stirring. The mixture was stirred for a minute and then filtered into a solution of 12 g Et_4NBr dissolved in 40 mL water. The yellow suspension was stirred for 10−15 min and allowed to stand for 10−15 min. The crude product was isolated by filtration and washed thoroughly with four 100 mL portions of water (till the washed solution became colorless), followed by three to four 50 mL portions of ethanol, two 50 mL portions of CS_2, and finally with two 100 mL portions of diethyl ether. The product was finally washed with three 10 mL portions of acetonitrile to remove $(Et_4N)_2Mo_2O_2S_9$ which was formed as a minor by product. The crude product was again washed with diethyl ether and dried under vacuum. The product could be used without further purification or was extracted with a minimal amount of dimethylformamide (DMF) (ca. 500 mL per 10 g of crude product), filtered, and was recrystallized by the addition of 1.5 volume of diethyl ether. Yield: 12 g. (65%). IR (KBr pellet): ν 932 (vs, Mo═O), 430 (w, Mo−S) cm^{-1}. λ_{max} (ϵ_M in M^{-1} cm^{-1}) in dimethylformamide: 316 (17 500), 400 (sh) nm.

$[Et_4N]_2[Mo^{IV}O(mnt)(S_4)]$ (2). To an acetonitrile solution (50 mL) of $(Et_4N)_2[Mo^{IV}O(S_4)_2]$ (**1**) (0.63g, 1 mmol) was added Na_2mnt (0.186 g, 1 mmol) followed by ∼3−5 mL of water. The solution was stirred for 75 min at room temperature when the solution colored red. After the removal of the precipitated elemental sulfur from the solution by filtration, diethyl ether was added to the filtrate to make it hazy. A golden yellow shiny product which was precipitated out was removed by filtration. To the red filtrate more ether was added to layer the solution, and this was allowed to stand overnight at 4 °C to yield red needle shaped diffraction quality crystals. The red crystals were collected and washed with isopropanol and ether. A second crop of these crystals was collected after allowing the mother liquor to stand at 4 °C by further layering with ether. Yield: 0.42 g (65%). Required for $C_{20}H_{40}MoN_4OS_6$: C 37.48, H 6.29, N 8.74, S 30.02%. Found: C 37.30, H 6.31, N 8.71, S 29.93%. IR (KBr pellet): ν 924 (Mo═O), 1481 (C═C), 2195, 2208 (C≡N), 2943, 2975 (aliphatic C—H) cm^{-1}. λ_{max} (ϵ_M in M^{-1} cm^{-1}) in acetonitrile: 334 (sh), 391 (5489) nm.

$[Et_4N]_2[Mo^{IV}O(mnt)(DMED)]$ (3). To an acetonitrile solution (50 mL) of $(Et_4N)_2[Mo^{IV}O(mnt)(S_4)]$ (**1**) (0.642 g, 1 mmol)was added dimethyl acetylenedicarboxylate (DMAD) (0.2 mL, 1.6 mmol) by constant stirring which was continued for 2 h at room temperature whereby an orange solution is formed along with the precipitation of sulfur. The precipitated sulfur was removed by filtration. To the filtrate diethyl ether was layered to create a cloudiness at the junction of the two solvents, and this was allowed to stand overnight at 4 °C to obtain pea-green needle shaped diffraction quality crystals. The pea-green crystals obtained from the orange solution were collected and washed with isopropanol and ether. Yield: 0.51 g (71%). Required for $C_{26}H_{46}MoN_4O_5S_4$: C 43.44, H 6.45, N 7.79, S 17.84%. Found: C 43.35, H 6.37, N 7.88, S 17.76%. IR (KBr pellet): ν 919 (Mo═O), 1483 (C═C), 1691 (symmetric C═O), 1720 (asymmetric C═O), 2188 (C≡N), 2948, 2986 (aliphatic C—H) cm^{-1}. λ_{max} (ϵ_M in M^{-1} cm^{-1}) in acetonitrile: 358 (9770), 422 (1590), 484 (393), 604 (221) nm.

$[Et_4N]_2[Mo^{IV}O(mnt)(bdt)]$ (4). To an acetonitrile solution (15 mL) of $(Et_4N)_2[Mo^{IV}O(mnt)(S_4)]$ (**1**) (0.1g, 0.16 mmol) was added benzenedithiol (0.02 mL, 0.17 mmol) with constant stirring. The solution was then stirred for 3 h at room temperature when the initial red color of the solution turned to green with the precipitation of sulfur. The precipitated sulfur was removed by filtration. To the filtrate diethyl ether was layered to bring cloudiness which was then allowed to stand overnight at 4 °C to yield pea-green needle shaped diffraction quality crystals. The pea-green crystals were collected and washed with isopropanol and ether. Yield: 0.07 g (69%). Required for $C_{26}H_{44}MoN_4OS_4$: C 47.83, H 6.79, N 8.58, S 19.65%. Found: C 47.74, H 6.71, N 8.63, S 19.71%. IR (KBr pellet): ν 921 (Mo═O), 1478 (C═C), 2187(C≡N), 2947, 2979 (aliphatic C—H) cm^{-1}. λ_{max} (ϵ_M in M^{-1} cm^{-1}) in acetonitrile: 301 (12 876), 337 (sh), 407 (2637), 628 (159) nm.

$[Et_4N]_2[Mo^{IV}O(mnt)(tdt)]$ (5). To an acetonitrile solution (10 mL) of $(Et_4N)_2[Mo^{IV}O(mnt)(S_4)]$ (**1**) (0.064g, 0.1 mmol) was added toluenedithiol (0.03 g, 0.19 mmol). The solution was stirred for 6 h at 60 °C and then 2 h at room temperature to get green solution. The resulting green solution was then concentrated to precipitate elemental sulfur. The precipitated elemental sulfur was removed by filtration. To the filtrate, diethyl ether was layered to bring cloudiness, and the mixture was allowed to stand overnight at 4 °C to yield green block shaped diffraction quality crystals. The green crystals were collected and washed with isopropanol and ether. Yield: 0.047 g (71%). Required for $C_{27}H_{46}MoN_4OS_4$: C 48.63, H 6.95, N 8.40, S 19.32%. Found: C 48.60, H 6.91, N 8.46, S 19.28%. IR (KBr pellet): ν 919 (Mo═O), 1477 (C═C), 2187 (C≡N), 2945, 2978 (aliphatic C—H) cm^{-1}. λ_{max} (ϵ_M in M^{-1} cm^{-1}) in acetonitrile: 304 (9042), 343 (sh), 405 (2033), 628 (258) nm.

X-ray Crystallography. Suitable diffraction quality crystals were selected from the homogeneous samples under polarizing microscope.

dx.doi.org/10.1021/ic4002576 | Inorg. Chem. 2013, 52, 5316−5327

Such selected crystals, each one from the complexes **2**, **3**, **4**, and **5**, were glued to glass fiber for the respective data collection by mounting on a BRUKER SMART APEX diffractometer. The instrument was equipped with a CCD area detector, and data were collected using graphite-monochromated Mo Kα radiation (λ = 0.710 69 Å) at low temperature (100 K). Cell constants were obtained from the least-squares refinement of three-dimensional centroids through the use of CCD recording of narrow ω rotation frames, completing almost all-reciprocal space in the stated θ range. All data were collected with SMART 5.628 (BRUKER, 2003), and were integrated with the BRUKER SAINT program.[15] The structure was solved using SIR97[16] and refined using SHELXL-97.[17] Crystal structures were viewed using ORTEP.[18] Full-matrix least-squares/difference Fourier cycles were performed which located the remaining non-hydrogen atoms. All non-hydrogen atoms were refined with anisotropic displacement parameters.

Kinetic Measurements. These experiments were performed in acetonitrile medium. The reductions of $(CH_3)_3N^+-O^-$ by complexes **3** and **4** were monitored by electronic spectroscopy using a Lambda 35 UV−vis spectrometer (Perkin −Elmer) with PCB 150/PTP-6 Peltier System. Because of the dependence of the dielectric of the medium and the concentration of H^+ present in the reaction mixture during the reduction of $((CH_3)_3N^+-O^-$ by **3**, we have used a fixed pH in all these measurements. We have carried out the kinetic experiments within the range of apparent pH 6−6.5 (in acetonitrile medium). The pH of the present measurement was maintained by adding proportional amount of glacial acetic acid into a solution of $(CH_3)_3N^+$-O^- in acetonitrile. Under such condition $(CH_3)_3N^+-O^-$ remains in the protonated form.[19] This protonated form is isolated by adding sodium tetraphenylborate in an aliquot of this mixture and adding water to precipitate out the salt, $[(CH_3)_3NOH]^+[B(Ph)_4]^-$. This protonated species instantly reacts with **3** or **4** in solvents like polar DMF or in relatively nonpolar DCM to yield quantitatively the corresponding oxidized species. For well behaved kinetics, such protonated substrate in the present case is important as free $(CH_3)_3N^+-O^-$ is sluggish to participate in such an oxo transfer reaction. The dissolution of pure $(CH_3)_3N^+-O^-$ (pK_a = 4.6) in water raises the pH of water due to the aquation to form basic ion pair, $[(CH_3)_3NOH]^+[OH]^-$. Crystalline TMANO is stable in the dihydrated form like $(CH_3)_3N^+-O^-\cdot 2H_2O$ and so inherently possesses $[(CH_3)_3NOH]^+[OH]^-$. It is interesting to note that the neutralization of the counteranion, $[OH]^-$, is crucial for a smooth oxo-transfer reaction. This can be achieved by adding any weak acid like benzoic acid or even by aspartic acid.[20] Native TMANOR performed optimally at pH 6.8,[21] and the amino acids present near the active site may scavenge the hydroxyl group from the approaching aquated substrate. As the native enzyme kinetics show well behaved saturation kinetics with a single substrate, the involvement of only one form of $(CH_3)_3N^+-O^-$ is ensured. The progress in the oxo transfer reaction between the reactant, $(CH_3)_3N^+-O^-$, and **3** at that apparent pH was monitored by electronic absorption spectroscopy. The appearance of tight isosbestic points at 351 and 368 nm on the reaction of $(CH_3)_3N^+-O^-$ with complex **3** showed the progress of a clean reaction. The electronic spectral profile of the final spectrum is similar to the electronic spectra of the reported dioxo Mo(VI) complexes.[8,9,22] The wavelength 532 nm for complex **3** was chosen to monitor the progress of reaction because at this wavelength the difference in the optical density of **3** and its corresponding dioxo complex is at a maximum. For all the kinetics measurements, first the solution of a particular concentration of complex **3** and $(CH_3)_3N^+-O^-$ in acetonitrile was prepared and then pH was adjusted at 6−6.5 by adding glacial acetic acid. The volume and concentration of the complex **3** and the substrate were adjusted in such a way that when they were mixed together the concentration of **3** remained always 1×10^{-4} M and the substrate concentration was varied in the range from 2.0×10^{-3} to 11.0×10^{-3} M. The progress of such a reaction was monitored by following the increase in absorbance as a function of time at 532 nm. Three kinetic runs were made for each of the substrate concentrations over the entire range of substrate concentration at 25 ± 1 °C under first-order conditions based on the substrate. Thus, the rate of the formation of dioxo complex from **3** that is the increase in the concentration of dioxo at time t was calculated from the absorbance at 532 nm using the equation $C_t = (A_\infty - A_t)/(\epsilon_2 - \epsilon_1)$, where C_t is the molar concentration of the dioxo complex at the time t, and ϵ_1 and ϵ_2 are the molar extinction coefficients of the complex **3** and its corresponding dioxo complex, respectively, at 532 nm. A_t is the absorbance of the reaction mixture at time t; A_∞ is the absorbance of the dioxo complex at the infinite time which is the absorbance of the completely oxidized product of **3**. This was calculated from the known value of concentration of **3** and ϵ_2 (spectroscopically observed when the dioxo complex is formed quantitatively; the same concentration of the dioxo complex should have formed at the time = ∞). Plots of ($-\ln C_t$) versus time were found to be linear, and from these k_{obs} values were calculated at each substrate concentration. Plot of $1/k_{obs}$ versus $1/[(CH_3)_3N^+-O^-]$ (Lineweaver−Burk plot) yielded the v_{max} and K_m values. Since three kinetic runs were carried out for each kinetic measurement, the mean value of the first-order rate constant and their standard deviations were computed. The rate constant values were then subjected to a conventional curve-fitting procedure (method of least-squares) to obtain the different plots.

Similarly the kinetic measurement for the complex **4** at fixed wavelength 521 nm has been carried out varying the substrate concentration in the range from 1.5×10^{-4} to 9×10^{-4} M. In this case the appearance of a tight isosbestic point at 344 nm during the progress of the oxo transfer reaction confirmed a clean reaction.

Thus, the reduction of $(CH_3)_3N^+-O^-$ was followed by observing the appearance of the 532 nm (in the case of **3**) and 521 nm bands (in the case of **4**), respectively. Tight isosbestic points at 351, 368 nm in the case of **3** and 344 nm in the case of **4** demonstrated that these oxo transfer reactions proceed cleanly to the completion of the reaction as shown in the eq 2:

$$[Mo^{IV}O(mnt)(DMED/bdt)]^{2-} + (CH_3)_3N^+-O^- + 2H^+ \rightarrow [Mo^{VI}O_2(mnt)(DMED/bdt)]^{2-} + (CH_3)_3N + H_2O \quad (2)$$

Computational Details. All calculations were performed using the Gaussian 03 (Revision B.04) package[23] on an IBM PC platform. The initial geometry was taken from the crystal structure, and gas phase single-point calculations were performed. The calculations were done supposing the zero electronic spin. The method (ROB3LYP) used was Becke's three parameter hybrid exchange functional,[24a] the nonlocal correlation provided by the Lee, Yang, and Parr expression.[24b] 6-31G*+ basis set[25] was used for C, H, N, S, and O atoms. The LANL2DZ basis set[26] and LANL2DZ pseudopotentials of Hay and Wadt[27] were used for the Mo atom. Molecular orbitals were visualized using "Gauss View". The assignment of the type of each MO was made on the basis of its composition and by visual inspection of its localized orbital. The low-lying singlet states (80 states) of complexes **2**, **3**, **4**, and **5** have been calculated on the basis of the crystal structure (nonoptimized) geometry of S_0 through a time-dependent density functional theory (TD-DFT)[28] approach using polarized continuum model (PCM) with the default parameters for acetonitrile.

For the reaction pathway studies all calculations were performed using the Gaussian 09 (Revision B.01) package[29] on a Linda platform. Transition states and saddle points were located by following a relaxed potential energy surface (PES) scan from reactants to intermediate and then to products. The substrate, $(CH_3)_3NO$ ($(CH_3)_3N^+-O^-$) or $\{(CH_3)_3NOH\}^+$, was placed at 3.5 Å from the molybdenum complex with the oxygen pointing toward the molybdenum atom. It is anticipated that the oxygen atom should finally reach to the molybdenum center from the cis position to the oxo group attached to the molybdenum center. The Mo−O(substrate) distance was then shortened in several steps with geometry optimization at each step while the remaining degrees of freedom were allowed to vary to detect transition states and saddle points using the polarized continuum model (PCM) with the default parameters for acetonitrile. Similarly, on scanning from intermediate to product, the $MoOH-N(CH_3)_3$ distance was shortened or $MoO-N(CH_3)_3$ distance was increased in the same way as described above. The optimized minima, transition states, and intermediates have been characterized by harmonic

dx.doi.org/10.1021/ic4002576 | Inorg. Chem. 2013, 52, 5316−5327

Scheme 1

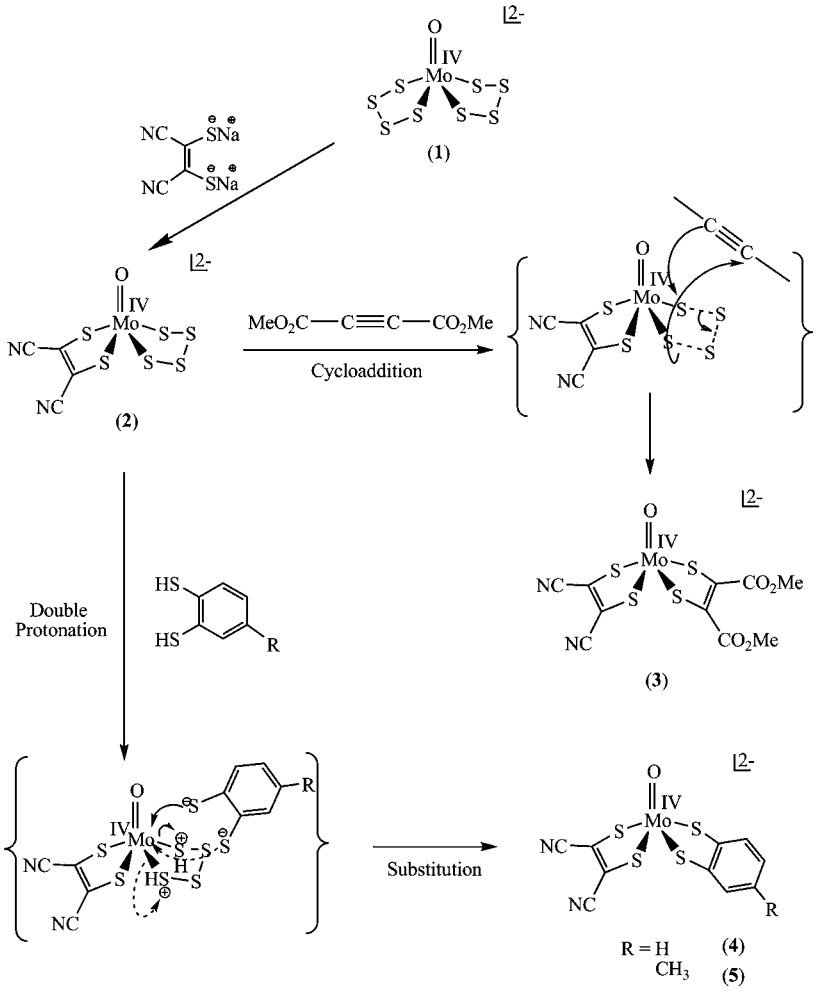

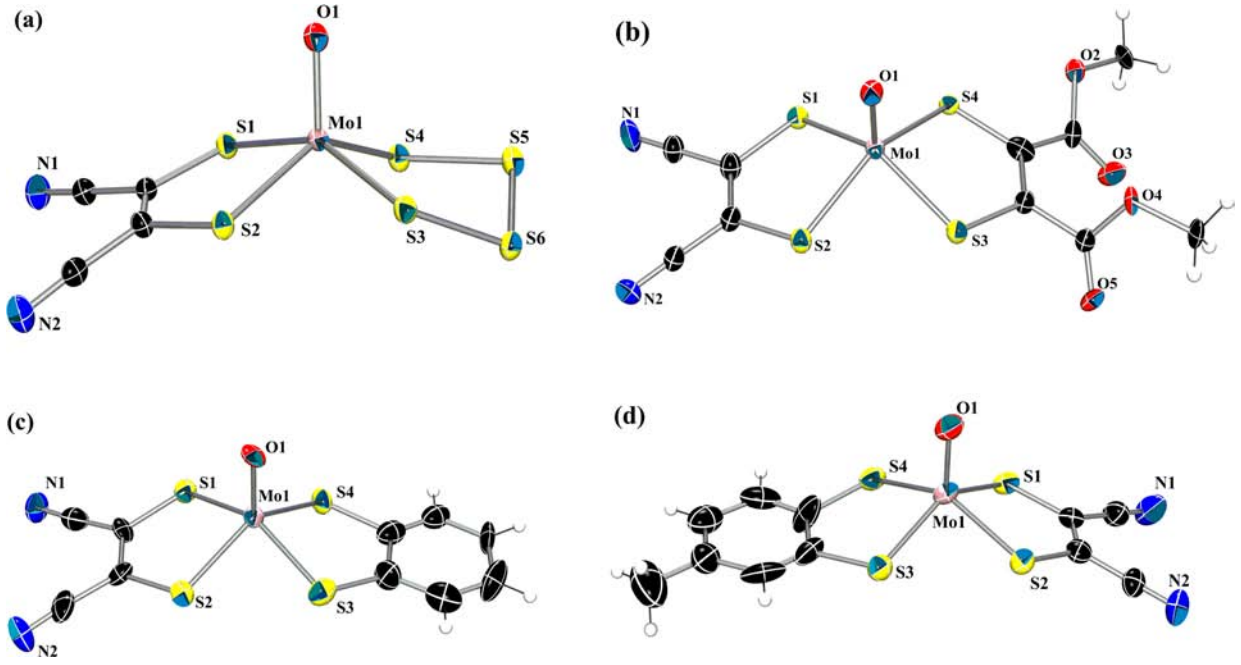

Figure 1. Structure (ORTEP view) of the anion of (a) $[Et_4N]_2[Mo^{IV}O(mnt)(S_4)]$ (**2**), (b) $[Et_4N]_2[Mo^{IV}O(mnt)(DMED)]$ (**3**), (c) $[Et_4N]_2[Mo^{IV}O(mnt)(bdt)]$ (**4**), and (d) $[Et_4N]_2[Mo^{IV}O(mnt)(tdt)]$ (**5**) showing 50% probability thermal ellipsoids with selected atom labeling scheme.

dx.doi.org/10.1021/ic4002576 | *Inorg. Chem.* 2013, 52, 5316−5327

Table 1. Crystallographic Data[a] for Complexes 2−5

	2	3	4	5
formula	$C_{20}H_{40}MoN_4OS_6$	$C_{26}H_{46}MoN_4O_5S_4$	$C_{26}H_{44}MoN_4OS_4$	$C_{27}H_{46}MoN_4OS_4$
fw	640.86	718.85	652.83	666.86
cryst syst	monoclinic	monoclinic	monoclinic	monoclinic
space group	$P2_1/c$	Pc	$P2_1/n$	$P2_1/n$
T (K)	100	100	100	100
Z	4	4	4	4
a, Å	11.336(5)	9.408(5)	8.605(5)	8.608(5)
b, Å	14.150(5)	11.503(5)	30.762(5)	30.806(5)
c, Å	18.252(5)	31.071(5)	11.638(5)	12.012(5)
α, deg	90.000(5)	90.000(5)	90.000(5)	90.000(5)
β, deg	91.852(5)	91.996(5)	90.002(5)	92.689(5)
γ, deg	90.000(5)	90.000(5)	90.000(5)	90.000(5)
V, Å^3	2926.2(18)	3361(2)	3081(2)	3182(2)
d_{calcd} (g/cm^3)	1.455	1.421	1.408	1.392
μ (mm^{-1})	0.896	0.678	0.723	0.701
θ range, deg	2.30−27.00	2.20−28.00	2.19−26.00	2.15−28.00
GOF (F^2)	1.143	1.097	1.223	1.068
R1[b] (wR2[c])	0.0399 (0.1476)	0.0669 (0.2442)	0.1282 (0.3076)	0.0983 (0.2323)

[a] Mo Kα radiation (λ = 0.710 69 Å). [b] $R1 = \sum||F_o| - |F_c||/\sum|F_o|$. [c] $wR2 = \{\sum[w(F_o^2 - F_c^2)^2]/\sum[w(F_o^2)^2]\}^{1/2}$.

Table 2. Selected Bond Distances (Å) for Complexes 2−5

	distances (Å)					
		from mnt		from other dithiolate		
complex	Mo═O(1)	Mo—S(1)	Mo—S(2)	Mo—S(3)	Mo—S(4)	displacement of Mo(1) from S_4 (dithiolene sulfur) mean plane
2	1.700(3)	2.421(12)	2.421(11)	2.343(12)	2.339(12)	0.753
3	1.703(8)	2.392(3)	2.394(4)	2.371(3)	2.388(3)	0.749
4	1.696(10)	2.401(4)	2.399(4)	2.367(4)	2.369(4)	0.741
5	1.690(6)	2.394(2)	2.401(2)	2.365(2)	2.366(3)	0.756

vibration frequency calculation with the same method and basis set where minima and intermediates have no imaginary frequency and transition state has one imaginary frequency. The relative energies reported have been corrected with zero point energies.

RESULTS AND DISCUSSIONS

Synthesis. The known $[Mo^{IV}O(S_4)_2]^{2-}$ complex anion[14] was used as the starting material to design the asymmetric bis dithiolene coordination. We used simple substitution of the coordinated S_4^{2-} by mnt^{2-}. Interestingly, irrespective of the stoichiometry of mnt^{2-} (1 or 2 equiv) used, only one S_4^{2-} ligand is replaced from **1** to yield **2** in aqueous acetonitrile medium .The synthesis of complexes **2**−**5** is schematically shown in Scheme1.

Complex **2** was briefly mentioned as unpublished work by Coucouvanis et al.[30]Complex **2** was previously structurally characterized and was obtained by a reaction between $\{[O{=}Mo^{VI}(S_2)_2]Cl\}^{1-}$ and Na_2mnt where substitution of the Cl^- by mnt^{2-} is accompanied by internal electron transfer concomitant with the oxidative coupling of the two S_2^{2-} ligands.[30]

To introduce a different dithiolene coordination to molybdenum in the $\{O{=}Mo^{IV}(S_4)(mnt)\}$ unit, we have employed two different synthetic routes. The first method is the cycloaddition of activated alkynes across the tetrasulfido moiety of Mo center (Scheme 1).[31] The other method involves direct displacement of the coordinated tetrasulfido (S_4^{2-}) group by protonated dithiol (Scheme 1).[32] Only 1 equiv of benzenedithiol is needed to form **4** at 25 °C; otherwise, excess benzenedithiol produces $[Mo^{IV}(mnt)(bdt)_2]^{2-}$. Excess ligand is used for the synthesis of **3** and **5** from **2**. Synthesis of **5** requires warming the reaction mixture.

Description of Structures. Suitable X-ray diffraction quality single crystals of complexes **2**−**5** were made according to the procedure described in the synthetic section. Crystal structures of the anionic part of the complexes **2**, **3**, **4**, and **5** are presented in Figure 1.

The presence of two counter monopositive cations in each crystal structure suggests an overall 2(−) charge on each of the anion of the complexes that is consistent with the assignment of the formal oxidation state of the molybdenum as IV. The Mo1 atom is coordinated by two sulfur atoms S1 and S2 of the mnt, a terminal oxo O1, and two sulfur atoms S3 and S4 from the varying dithiolene group. The average Mo−S (2.33−2.42 Å) distance in these complexes is quite similar to those observed for the other related molybdenum bis(dithiolene) complexes.[10,22,33−37] There is a small variation in the Mo═O bond distance, and generally, the Mo═O bond is longer within the series (Table 2) compared with the short Mo═O bond (1.67 Å) in symmetric bis-dithiolate complex, $[Et_4N]_2[Mo^{IV}O(mnt)_2]$. Mo−$S_{mnt}$ exhibits slightly longer bond distances than those from the other Mo−$S_{otherdithiolate}$ used. As expected the Mo atom is displaced 0.74−0.75 Å above the mean S_4 plane composed of S1, S2, S3, and S4 in all these complexes. In these the bond angle of S1−Mo1−S3 is not close to that of S2−Mo1−S4, and the four different bond angles of O1−Mo1−S1, O1−Mo1−S2, O1−Mo1−S3, and O1−Mo1−S4 indicate that the Mo1 center adopts a square pyramidal geometry. In complex **2** (Figure 1), the S4, S5, S6, and S3 atoms of the tetrasulfido group form a zigzag structure where the torsion

dx.doi.org/10.1021/ic4002576 | Inorg. Chem. 2013, 52, 5316−5327

angle defined by S4−S5−S6−S3 is 45.1°. The crystal of **3** contains two crystallographically independent complex anions and four Et_4N cations in the lattice. The two anions are chemically identical although the geometrical parameters of both are marginally different and the structure of one of the complex anion is shown in Figure 1.

The leading structural parameters for the synthesized complexes have been collected in Table 1. The selected bond distances and angles are listed in Tables 2 and 3.

Table 3. Selected Angles (deg) for Complexes 2−5

	complex			
angle (deg)	2	3	4	5
O1−Mo1−S1	103.26(10)	110.5(3)	109.2(3)	110.4(2)
O1−Mo1−S2	112.74(10)	106.2(3)	105.2(4)	105.7(2)
O1−Mo1−S3	106.93(10)	108.0(3)	110.8(4)	110.4(2)
O1−Mo1−S4	111.00(10)	108.5(3)	107.3(4)	107.5(2)
S1−Mo1−S3	149.31(4)	141.51(10)	140.06(13)	139.15(8)
S2−Mo1−S4	135.98(4)	145.27(9)	147.39(13)	146.74(8)

UV−Vis Spectroscopy. The electronic spectra of **2**, **3**, **4**, and **5** are presented in Figure 2, and the UV−vis absorption

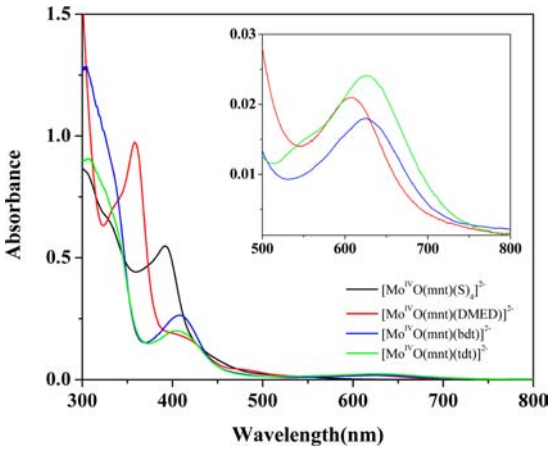

Figure 2. UV−vis absorption spectra (10^{-4} M in acetonitrile) of $[Et_4N]_2[Mo^{IV}O(mnt)(S_4)]$ (**2**) (black), $[Et_4N]_2[Mo^{IV}O(mnt)$-(DMED)] (**3**) (red), $[Et_4N]_2[Mo^{IV}O(mnt)(bdt)]$ (**4**) (blue), and $[Et_4N]_2[Mo^{IV}O(mnt)(tdt)]$ (**5**) (green). Inset shows absorbance around 600 nm.

Table 4. UV−Vis Absorption Data (in Acetonitrile) for Complexes 2−5

complex	λ_{max} in nm (ε)			
2	334 (sh)	391 (5489)	449 (sh)	
3	358 (9770)	422 (1590)	484 (393)	604 (221)
4	301 (12 876)	337 (sh)	407 (2637)	628 (159)
5	304 (9042)	343 (sh)	405 (2033)	628 (258)

maxima of these are given in Table 4. The intense high-energy transitions around 300−400 nm are normally associated with the internal ligand transition. The transitions occurring at longer wavelengths are tentatively assigned as sulfido (from dithiolene) and tetrasulfido to Mo charge-transfer absorptions.

Electrochemistry. The electrochemical properties of these complexes are investigated by cyclic voltammetry. Cyclic voltammetric traces for complexes **2**−**5** are shown in Figure 3 and investigated by both the oxidative and reductive scans.

Complex **2** showed two irreversible oxidations typical for sulfur rich species.[14b,32,38,39] The low potential oxidation at E_{pa} = 0.24 V is tentatively assigned for the oxidation of coordinated tetrasulfido moiety, and the oxidation at the higher potential of above 0.7 V is related to the oxidation of the dithiolene ligand; such value is common to all other dithiolene complexes.[14,40] The first irreversible reduction at E_{pc} = −0.78 V (Figure 3) may be related to the reduction of the tetrasulfido moiety in forming a radical ion. For all the complexes an irreversible reduction at around E_{pc} = −1.85 V (Figure 3) may be related to the reduction of coordinated maleonitriledithiolene ligand.[40,41] The assignments of these electrochemical data are tentative and based on the reported work of similar complexes and were not characterized spectroscopically. In addition, complexes **3**, **4**, and **5** exhibit reversible redox couple at $E_{1/2}$ = 0.18 V (ΔE = 80 mV), $E_{1/2}$ = 0.00 V (ΔE = 68 mV), and $E_{1/2}$ = −0.032 V (ΔE = 70 mV), respectively (Figure S5). These couples are assignable to Mo(IV)/Mo(V) couples (*vide infra* (Figure 7)). A comparison (Figure 4) among **3**, **4**, and **5** indicates that the electronic effects contribute to the redox potential change through the conjugation between the π orbital of C═C group and the pπ orbital of sulfur atom. The reversible peak (Figure 4) shifts toward zero potential as the dithiolene group becomes more electron donating. Thus, complex **5** is more easily oxidizable, i.e., more reducing in nature.

Trimethylamine-N-oxide Reduction Involving Oxygen Atom Transfer Reaction. Complexes **3**, **4**, and **5** are found to reduce $(CH_3)_3N^+-O^-$ to $(CH_3)_3N$. $(CH_3)_3N^+-O^-$ reduction by complexes **3**, **4**, and **5** in acetonitrile medium was monitored by UV−vis spectroscopy, and the progress of these reactions is shown in Figure 5 (Figures S6 and S7).

The reaction of complex **3** with $(CH_3)_3N^+-O^-$ when monitored by UV−vis spectroscopy showed a clean reaction with tight isosbestic points at 351 and 368 nm, respectively (Figure S6), with the formation of a new absorption band at 532 nm. This new band is due to the formation of the oxidized species (inset in Figure S6).

Similarly, the reaction of complex **4** or **5** with $(CH_3)_3N^+-O^-$ when monitored by UV−vis spectroscopy showed a clean oxo transfer reaction with tight isosbestic point at 344 nm (Figure 5) or at 351 nm (Figure S7), respectively, and with the formation of a new absorption band at 521 or at 551 nm, respectively, which is due to the formation of the respective oxidized species (insets in Figure 5 and Figure S7).

Kinetics of Trimethylamine-N-oxide Reduction. The oxygen atom transfer reaction from $(CH_3)_3N^+-O^-$ to **3** and **4** in acetonitrile medium was spectrophotometrically monitored at 25 °C. Details of the kinetic experiments have been described in the section entitled as Kinetic Measurements. These reactions were found to be first-order with the respective Mo(IV) complexes indicated by the linearity of the plots of ($-\ln C_t$) versus time from which k_{obs} values were calculated at each substrate concentration. These plots of k_{obs} versus $[(CH_3)_3N^+-O^-]$ were found to be similar to the substrate saturation kinetics (Michaelis−Menten kinetics) exhibited by the native enzymes and were shown in Figure 6 and Figure S8 along with the corresponding Lineweaver−Burk plots.

dx.doi.org/10.1021/ic4002576 | *Inorg. Chem.* 2013, 52, 5316−5327

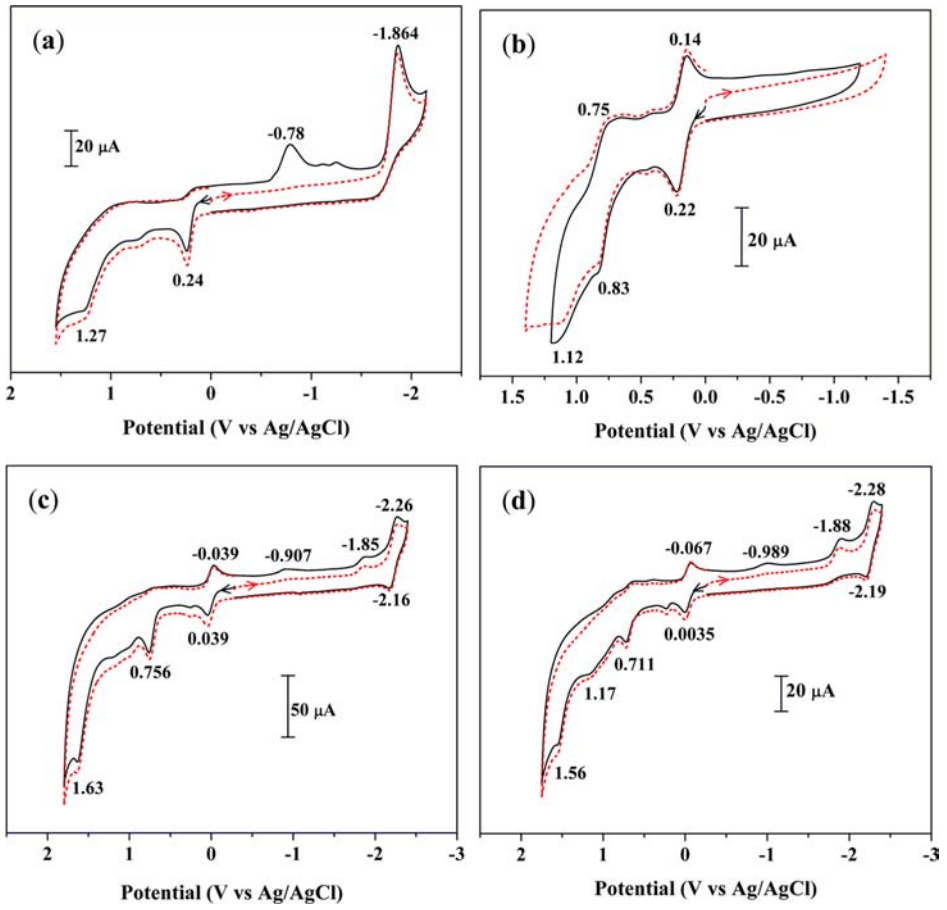

Figure 3. Cyclic voltammetric traces (scan rate = 100 mV/s) for (a) $[Et_4N]_2[Mo^{IV}O(mnt)(S_4)]$ (**2**), (b) $[Et_4N]_2[Mo^{IV}O(mnt)(DMED)]$ (**3**), (c) $[Et_4N]_2[Mo^{IV}O(mnt)(bdt)]$ (**4**), and (d) $[Et_4N]_2[Mo^{IV}O(mnt)(tdt)]$ (**5**) in acetonitrile; oxidative scan (black solid line) and reductive scan (red dotted line).

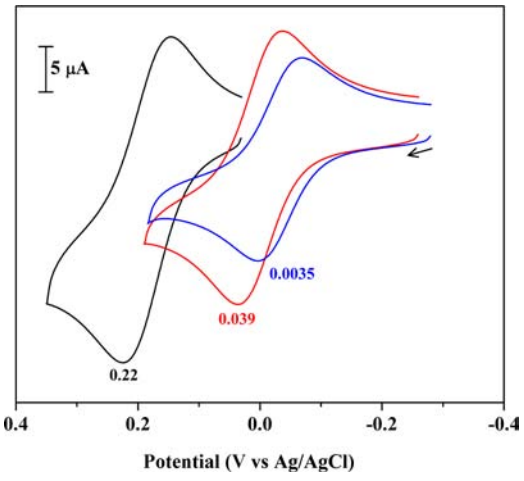

Figure 4. Reversible redox couple for complexes $[Et_4N]_2[Mo^{IV}O(mnt)(DMED)]$ (**3**) (black), $[Et_4N]_2[Mo^{IV}O(mnt)(bdt)]$ (**4**) (red), and $[Et_4N]_2[Mo^{IV}O(mnt)(tdt)]$ (**5**) (blue).

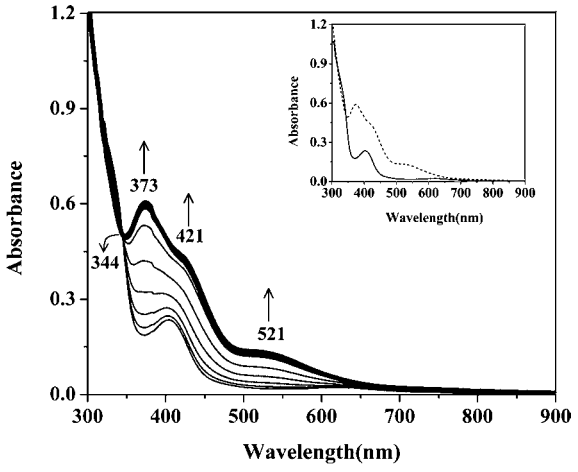

Figure 5. Spectral changes in the reaction of 1×10^{-4} M of $[Et_4N]_2[Mo^{IV}O(mnt)(bdt)]$ (**4**) with 4×10^{-4} M of $(CH_3)_3N^+-O^-$ in acetonitrile at 25 °C. Scan rate = 2 s/scan. Inset: spectra of **4** (solid line) and its oxidized form (dotted line).

The kinetic parameters are presented in Tables 5, S2, and S3. Complex **4** showed larger v_{max} value than that of complex **3**. Kinetic investigations have not been performed with complex **5**.

The oxo-transfer reaction of $(CH_3)_3N^+-O^-$ by these complexes (Figures 5, S6, and S7) were presented in Scheme 2. The reaction pathway studies are then followed by the DFT level of calculation (*vide infra*).

Density Functional Theory Calculation. The reactivity of the synthesized complexes **3**, **4**, and **5** toward trimethylamine-N-oxide reduction has been followed by gas phase single point energy calculation. For this, the respective geometry was obtained from the individual crystal structure. Details of these

dx.doi.org/10.1021/ic4002576 | *Inorg. Chem.* 2013, 52, 5316−5327

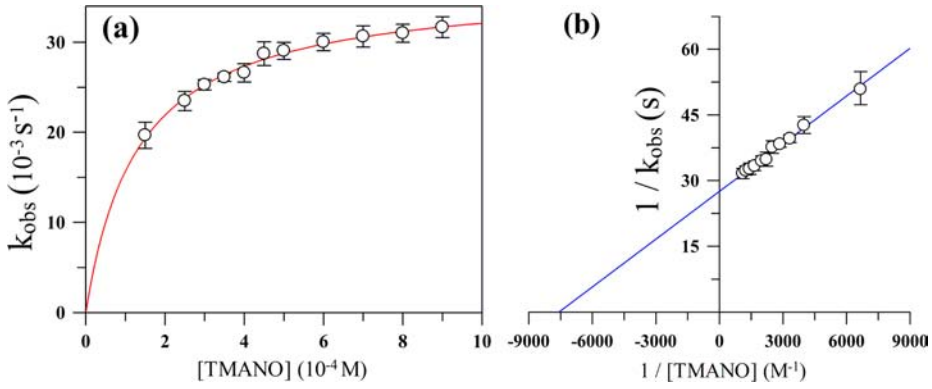

Figure 6. Dependence of the rate of reaction of (a) $[Et_4N]_2[Mo^{IV}O(mnt)(bdt)]$ (**4**) with 1.5–9.0 equiv of TMANO in acetonitrile at 25 °C on [TMANO]. (b) Corresponding Lineweaver–Burk plot of part a.

Table 5. Kinetics Results for Trimethylamine-N-oxide Reduction by Complexes 3 and 4[a]

complex	K_m (M)	v_{max} (s^{-1})
$[Et_4N]_2[Mo^{IV}O(mnt)(DMED)]$ (**3**)	4.9×10^{-3} M	9.2×10^{-3}
$[Et_4N]_2[Mo^{IV}O(mnt)(bdt)]$ (**4**)	1×10^{-4}	3.6×10^{-2}

[a] K_m, Michaelis constant; v_{max}, maximum velocity .

Scheme 2. Schematic Representation for the Enzymatic Reduction of Trimethylamine-N-oxide

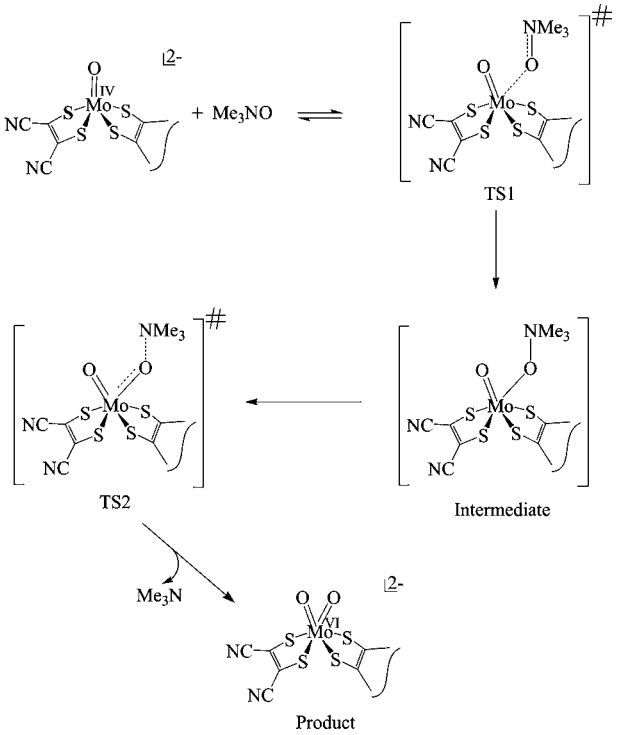

theoretical calculations are described in the section entitled as Computational Details.

The molecular orbital responsible in oxygen atom transfer reaction with trimethylamine-N-oxide should be the HOMO of the respective complexes. The HOMO of $\{[Mo^{IV}O(mnt)(DMED)]^{2-}\}$ (Figure 7) is found to be predominantly metal based (mainly metal d_{xy}) which is responsible for its ability to take part in the reduction of trimethylamine-N-oxide to trimethylamine. The complexes, $\{[Mo^{IV}O(mnt)(bdt)]^{2-}\}$ and $\{[Mo^{IV}O(mnt)(tdt)]^{2-}\}$ (Figure 7), show a similar trend which

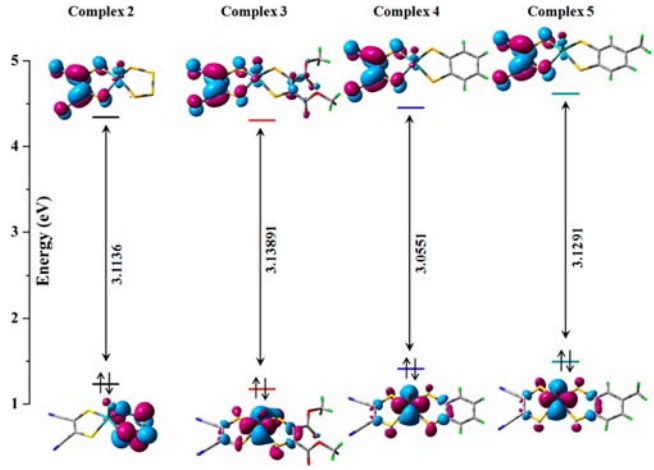

Figure 7. Relative energy of the selected MOs [HOMO (bottom) and LUMO (top)] in **2**, **3**, **4**, and **5**. Isosurface cut off value = 0.04. Color code for atoms: cyan, Mo; yellow, sulfur; blue, nitrogen; gray, carbon; green, hydrogen.

can be attributed to the ability of the respective Mo(IV) center to react with trimethylamine-N-oxide.

The stability and electrochemical behavior of these complexes can also be rationalized in the light of relative energy levels of these molecular orbitals. The stability of the complex **3** in comparison to the stability of other complexes is reflected by its relatively lower energy HOMO (Figure 7) compared to that in **2**, **4**, or **5**.

Furthermore, the HOMO of complex **2** is ligand centered. An oxidation at E_{pa} = 0.24 V in the case of **2** can be attributed to its low lying ligand centered HOMO (Figure 7). In contrast, the respective HOMOs of **3**, **4**, or **5** are metal centered. An oxidation at $E_{1/2}$ = 0.18 V, $E_{1/2}$ = 0.00 V, and $E_{1/2}$ = −0.032 V (vs Ag/AgCl) in the case of **3**, **4**, and **5**, respectively, follows their relative energy level of the metal centered HOMOs (Figure 7).

The TD-DFT calculations (Figures 8 and S9–S15, Tables S4–S7) showed that the intense absorption band in the ultraviolet region is mainly due to LLCT (ligand-to-ligand charge-transfer), i.e., π–π^* transitions of the ligands, while the bands that extend into the visible region correspond to the excitations to ML′LCT (metal ligand-to-ligand charge transfer) and MLCT (metal-to-ligand charge-transfer) for complex **3**, mixed LLCT (ligand-to-ligand charge-transfer), i.e., π–π^*, and MLCT for complexes **4** and **5**, respectively

dx.doi.org/10.1021/ic4002576 | Inorg. Chem. 2013, 52, 5316–5327

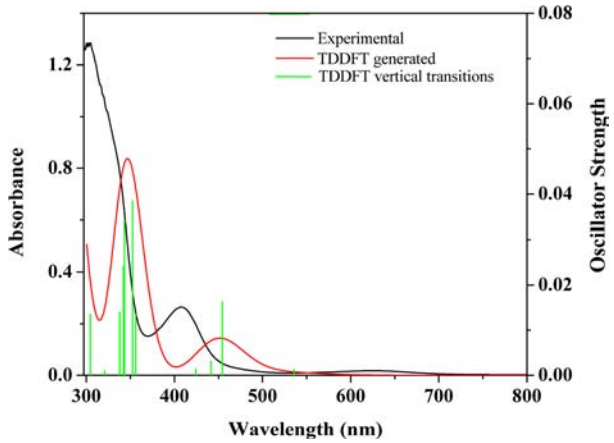

Figure 8. Experimental (10^{-4} M in acetonitrile; black) UV–vis of the complex $[Et_4N]_2[Mo^{IV}O(mnt)(bdt)]$ (**4**), and TD-DFT (red) UV–vis and TD-DFT vertical excitations (green sticks) of the complex anion of **4**.

The oxygen atom transfer reaction from $(CH_3)_3N^+-O^-$ to $[Mo^{IV}O(mnt)(bdt)]^{2-}$ for the overall oxidation of Mo^{IV} to Mo^{VI} as calculated by DFT is exothermic by ~103 kcal/mol (Figure 9). When $(CH_3)_3N^+-O^-$ enters the coordination sphere of the Mo, the starting square pyramidal complex changes to distorted octahedral geometry. A transition state was located at a Mo–$ON(CH_3)_3$ distance of ~3 Å (Figure 9 and Table S10) with energy ~4 kcal/mol above the starting point. In the transition state one of the sulfur atoms is moved from its position to allow access for the entering oxygen atom. The N–O bond in TMANO is now elongated (1.388 Å) compared to that at the starting point (1.362 Å). Upon further reduction of the Mo–$ON(CH_3)_3$ distance, an intermediate was found with a Mo–$ON(CH_3)_3$ distance of ~2.2 Å, and the energy 4.7 kcal/mol is below the energy of the starting point. The trans influence of the oxo ligand makes one of the Mo–S bonds (trans to the Mo═O) of the mnt ligand in the intermediate longer than the corresponding Mo—S bond trans to the entering oxygen atom of $(CH_3)_3N^+-O^-$. Upon increasing the MoO–$N(CH_3)_3$ distance from the intermediate structure, a second TS was located at an O–N bond distance of 1.68 Å and a Mo–$ON(CH_3)_3$ distance of 2.15 Å. This transition state (TS) is 1.7 kcal/mol below the starting point energy. A similar pathway has been documented.[42]

It is important to note that, in the presence of $\{(CH_3)_3NOH\}^+$ as the substrate, the reaction proceeds via one transition state followed by an intermediate (Figure 10 and Table S11).

Interestingly, the activation energy required for the transition state is slightly higher than (5.5 kcal/mol) that required for the unprotonated form. Also, the product released state is destabilized by −97.7 kcal/mol in energy compared to that (−102.9 kcal/mol) from the unprotonated form. Energetically, the magnitude of such a difference is not significant. It is suggested that the aliphatic N-oxides (like TMANO) are more readily protonated and its protonation precedes reduction.[43] The computed energy level difference by DFT between protonated and unprotonated forms of the substrate, TMANO, differs around 5 kcal/mol, and such a small energy difference is roughly equal to the a hydrogen bond energy. In native protein the extensive hydrogen bond network around the active site may decisively control the approaching zwitterionic TMANO favoring the formation of hydrogen bonded enzyme–substrate adduct for a smooth enzymatic oxo transfer reaction.

The electronic spectral profile of the *in situ* generated dioxo is similar to that of the TDDFT generated spectrum of the optimized dioxo complex which confirms that the product is none other than the dioxo species (Figures 11, S16, and S17).

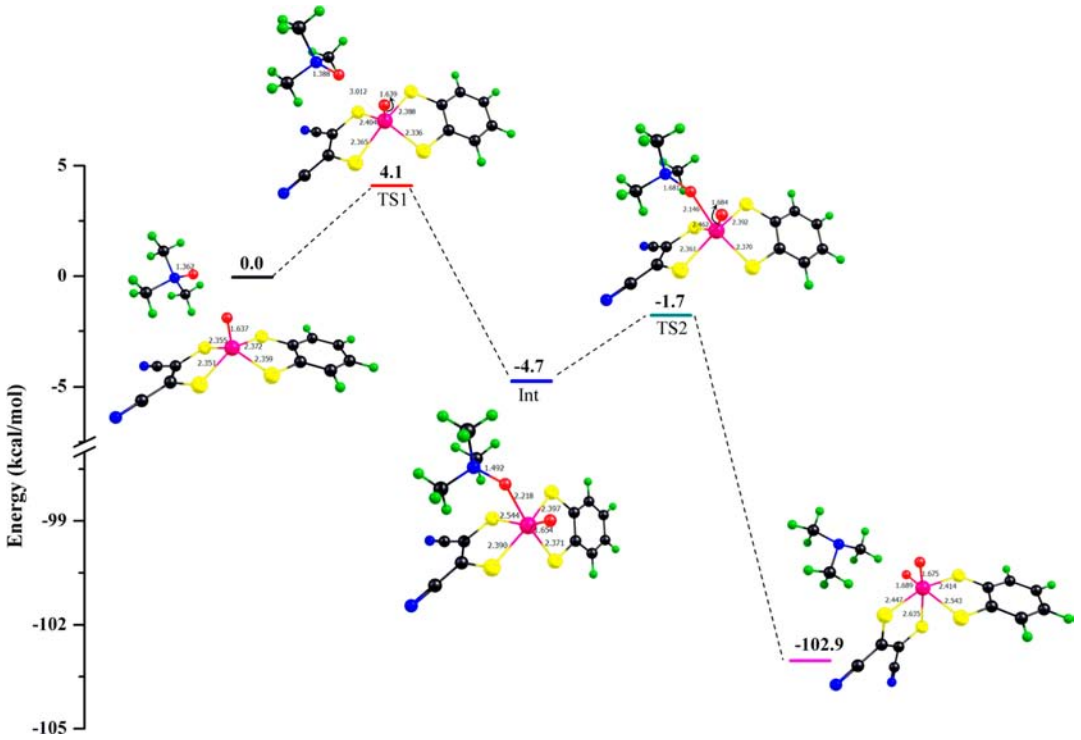

Figure 9. Energy profile for the reaction between the complex anion of $[Et_4N]_2[Mo^{IV}O(mnt)(bdt)]$ (**4**) and TMANO.

dx.doi.org/10.1021/ic4002576 | *Inorg. Chem.* 2013, 52, 5316–5327

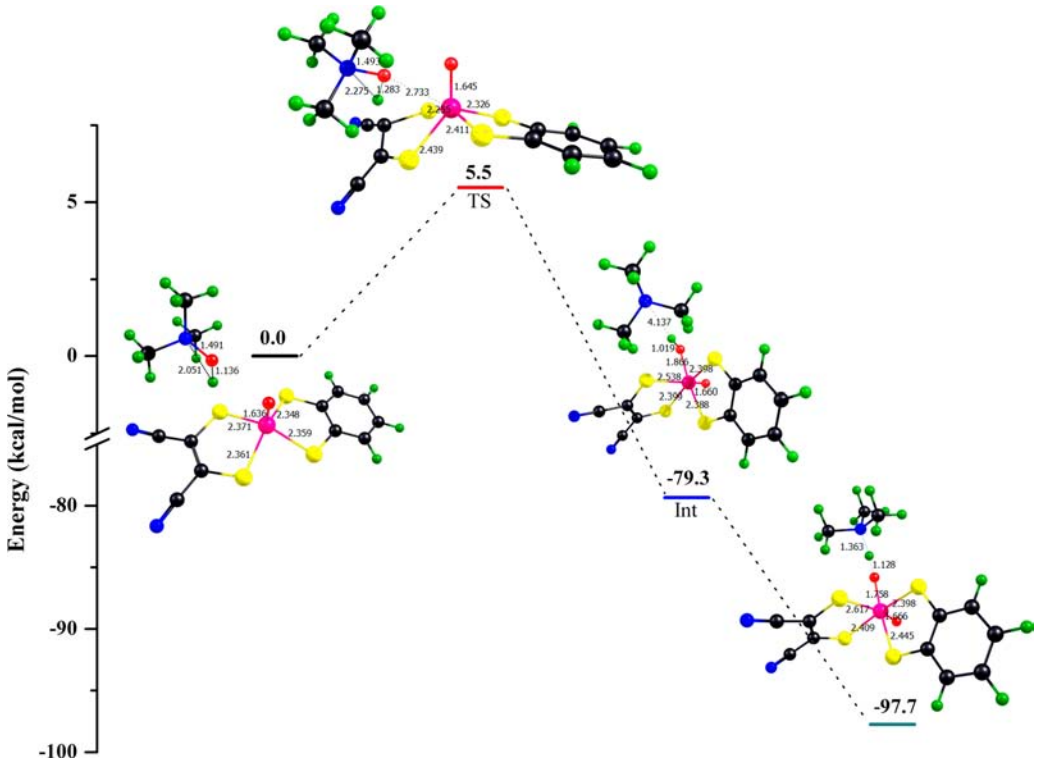

Figure 10. Energy profile for the reaction between the complex anion of $[Et_4N]_2[Mo^{IV}O(mnt)(bdt)]$ (**4**) and $\{(CH_3)_3NOH\}^+$.

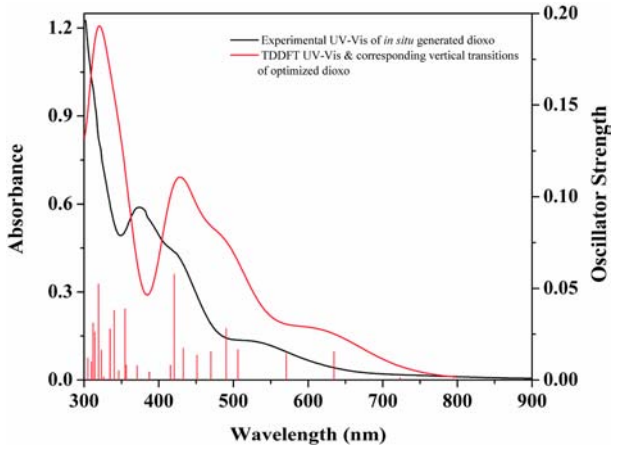

Figure 11. Experimental UV−vis in acetonitrile (black) of the *in situ* generated dioxo, and TD-DFT (red) UV−vis absorption spectra and TD-DFT vertical excitations (red sticks) of optimized product obtained from the reaction pathway between the complex anion of $[Et_4N]_2[Mo^{IV}O(mnt)(bdt)]$ (**4**) and $(CH_3)_3N^+-O^-$.

CONCLUSIONS

This work provides a detailed study of two analogue systems of trimethylamine-N-oxide reductase involved in the reduction of the relevant substrate, trimethylamine-N-oxide. These complexes possess asymmetric dithiolene ligands to simulate the two different pterin coordinations (P and Q) in DMSO reductase family of enzymes. The analogue systems are shown to reduce trimethylamine-N-oxide, and such reaction followed saturation kinetics (Michaelis−Menten) similar to the native enzyme.

DFT study of the reaction pathway revealed that in the presence of acidic environment the substrate in protonated form reacts via one transition state followed by an intermediate. But, in the absence of acid the reaction proceeds via two successive transition states along with an intermediate. Along the reaction pathway a Mo−O bond is gradually formed at the expense of N−O bond in $(CH_3)_3N^+-O^-$ or $\{(CH_3)_3NOH\}^+$ that is gradually weakened. There is also a structural change from the starting square pyramidal mono-oxo complex to the distorted octahedral dioxo complex. The native TMANO reductase possesses an elongated Mo−OR (serine residue), and the model complexes possess a stable Mo═O bond. It is known that a short Mo═O bond (1.67 Å) in $[Et_4N]_2[Mo^{IV}O(mnt)_2]$ is elongated (1.71 Å) in $[PyH]_2[Mo^{IV}O(mnt)_2]$ due to hydrogen bonding to enable its reaction toward TMANO.[34a] The present complexes each with two different dithiolene ligands control the Mo═O bond (Table 2, Table S1) spontaneously to elongate to close to ∼1.70 (Å) suggesting the unique role in asymmetric dithiolene coordination. Such a longer Mo═O bond may even be protonated under favorable pH condition to create a virtual Mo−OR (a longer Mo−O^- bond) situation where −OR represents the serine residue in the native protein. In addition it is suggested that the protonation of zwitterionic TMANO precedes reduction,[43] and therefore, it is possible that the protonated TMANO may be the substrate of choice. The computed energy levels by DFT between protonated and unprotonated forms of the substrate TMANO differ around 5 kcal/mol, and such a difference is really small to discard the possibility of its protonated form as the substrate. This energy difference is roughly equal to one hydrogen bond energy which may be compensated by the interaction with the hydrogen bonded network present in the active site in forming a hydrogen bonded enzyme−substrate adduct for a smooth enzymatic oxo transfer reaction.

dx.doi.org/10.1021/ic4002576 | *Inorg. Chem.* 2013, 52, 5316−5327

■ ASSOCIATED CONTENT

Supporting Information

Infrared spectra, kinetics data, optimized coordinates, and results of DFT and TDDFT calculations. Crystallographic data in CIF format. This material is available free of charge via the Internet at http://pubs.acs.org.

■ AUTHOR INFORMATION

Corresponding Author

*E-mail: abya@iitk.ac.in.

Notes

The authors declare no competing financial interest.

■ ACKNOWLEDGMENTS

G. M. and M. B. thank the Council of Scientific and Industrial Research (CSIR), New Delhi, for the award of doctoral fellowships, and S. S. thanks the Department of Science and Technology (DST), New Delhi, for generous funding on molybdenum enzymes.

■ REFERENCES

(1) Barrett, E. L.; Kwan, H. S. *Annu. Rev. Microbiol.* **1985**, *39*, 131−149.

(2) Mitchell, S. C.; Smith, R. L. *Drug. Metab. Dispos.* **2001**, *29*, 517−521.

(3) Hille, R. *Chem. Rev.* **1996**, *96*, 2757−2816.

(4) Czjzek, M.; Dos Santos, J. P.; Pommier, J.; Giordano, G.; Mejean, V.; Haser, R. *J. Mol. Biol.* **1998**, *284*, 435−447.

(5) Li, H. K.; Temple, C.; Rajagopalan, K. V.; Schindelin, H. *J. Am. Chem. Soc.* **2000**, *122*, 7673−7680.

(6) Zhang, L.; Nelson, K.; Rajagopalan, K.; George, G. *Inorg. Chem.* **2008**, *47*, 1074−1078.

(7) (a) Iobbi-Nivol, C.; Pommier, J.; Simala-Grant, J.; Mejean, V.; Giordano, G. *Biochim. Biophys. Acta* **1996**, *1294*, 77−82. (b) Johnson, K. E.; Rajagopala, K. V. *J. Biol. Chem.* **2001**, *276*, 13178−13185.

(8) (a) Oku, H.; Ueyama, N.; Kondo, M.; Nakamura, A. *Inorg. Chem.* **1994**, *33*, 209−216. (b) Ueyama, N.; Oku, H.; Kondo, M.; Okamura, T.; Yoshinaga, N.; Nakamura, A. *Inorg. Chem.* **1996**, *35*, 643−650. (c) Lim, B. S.; Sung, K. M.; Holm, R. H. *J. Am. Chem. Soc.* **2000**, *122*, 7410−7411.

(9) Baba, K.; Okamura, T.; Suzuki, C.; Yamamoto, H.; Yamamoto, T.; Ohama, M.; Ueyama, N. *Inorg. Chem.* **2006**, *45*, 894−901. Sugimoto, H.; Tatemoto, S.; Suyama, K.; Miyake, H.; Itoh, S.; Dong, C.; Yang, J.; Kirk, M. L. *Inorg. Chem.* **2009**, *48*, 10581−10590.

(10) Sugimoto, H.; Tatemoto, S.; Suyama, K.; Miyake, H.; Itoh, S.; Dong, C.; Yang, J.; Kirk, M. L. *Inorg. Chem.* **2009**, *48*, 10581−10590.

(11) (a) Garton, S. D.; Hilton, J.; Oku, H.; Crouse, B. R.; Rajagopalan, K. V.; Johnson, M. K. *J. Am. Chem. Soc.* **1997**, *119*, 12906−12916. (b) Kirk, M. L.; Helton, M. E.; McNaughton, R. L. *Prog. Inorg. Chem.* **2004**, *52*, 111−212. (c) McNaughton, R. L.; Lim, B. S.; Knottenbelt, S. Z.; Holm, R. H.; Kirk, M. L. *J. Am. Chem. Soc.* **2008**, *130*, 4628−4636. (d) Webster, C. E.; Hall, M. B. *J. Am. Chem. Soc.* **2001**, *123*, 5820−5821.

(12) Majumdar, A.; Sarkar, S. *Coord. Chem. Rev.* **2011**, *255*, 1039−1054 and references therein.

(13) Stiefel, E. I.; Bennett, L. E.; Dori, Z.; Crawford, T. H.; Simo, C.; Gray, H. B. *Inorg. Chem.* **1970**, *9*, 281−286.

(14) (a) Ansari, M. A.; Chandrasekaran, J.; Sarkar, S. *Inorg. Chim. Acta* **1987**, *133*, 133−136. (b) Hadjikyriacou, A. I.; Coucouvanis, D. *Inorg. Chem.* **1989**, *28*, 2169−2177.

(15) *SAINT, version 5.6*; Bruker AXS Inc.: Madison, WI, 2000.

(16) Altomare, A.; Burla, M. C.; Camalli, M.; Cascarano, G. L.; Giacovazzo, C.; Guagliardi, A.; Moliterni, A. G. G.; Polidori, G.; Spagna, R. *J. Appl. Crystallogr.* **1999**, *32*, 115−119.

(17) Sheldrick, G. M. *SHELX97. Programs for Crystal Structure Analysis (Release 97−2)*; University of Göttingen: Göttingen, Germany, 1997.

(18) Farrugia, L. J. *J. Appl. Crystallogr.* **1997**, *30*, 565−566.

(19) Pawlak, Z.; Tusk, M.; Kuna, S.; Strohbusch, F.; Fox, M. F. *J. Chem. Soc., Faraday Trans. 1* **1984**, *80*, 1757−1768.

(20) $(CH_3)_3N^+-O^-$ once coordinated in the complex, $[(CH_3)_3NOZnTPP]$ (TPP = tetraphenyl porphyrin), readily acts as oxo-transfer reagent thus implying that protonated form is not mandatory for a smooth reaction, to be published separately.

(21) Dos Santos, J.; Iobbi-Nivol, C.; Couillault, C.; Giordano, G.; Mejean, V. *J. Mol. Biol.* **1998**, *284*, 421−433.

(22) Das, S. K.; Chaudhury, P. K.; Biswas, D.; Sarkar, S. *J. Am. Chem. Soc.* **1994**, *116*, 9061−9070.

(23) Frisch, M. J.; Trucks, G. W.; Schlegel, H. B.; Scuseria, G. E.; Robb, M. A.; Cheeseman, J. R.; Montgomery, J. A., Jr.; Vreven, T.; Kudin, K. N.; Burant, J. C.; Millam, J. M.; Iyengar, S. S.; Tomasi, J.; Barone, V.; Mennucci, B.; Cossi, M.; Scalmani, G.; Rega, N.; Petersson, G. A.; Nakatsuji, H.; Hada, M.; Ehara, M.; Toyota, K.; Fukuda, R.; Hasegawa, J.; Ishida, M.; Nakajima, T.; Honda, Y.; Kitao, O.; Nakai, H.; Klene, M.; Li, X.; Knox, J. E.; Hratchian, H. P.; Cross, J. B.; Bakken, V.; Adamo, C.; Jaramillo, J.; Gomperts, R.; Stratmann, R. E.; Yazyev, O.; Austin, A. J.; Cammi, R.; Pomelli, C.; Ochterski, J. W.; Ayala, P. Y.; Morokuma, K.; Voth, G. A.; Salvador, P.; Dannenberg, J. J.; Zakrzewski, V. G.; Dapprich, S.; Daniels, A. D.; Strain, M. C.; Farkas, O.; Malick, D. K.; Rabuck, A. D.; Raghavachari, K.; Foresman, J. B.; Ortiz, J. V.; Cui, Q.; Baboul, A. G.; Clifford, S.; Cioslowski, J.; Stefanov, B. B.; Liu, G.; Liashenko, A.; Piskorz, P.; Komaromi, I.; Martin, R. L.; Fox, D. J.; Keith, T.; Al-Laham, M. A.; Peng, C. Y.; Nanayakkara, A.; Challacombe, M.; Gill, P. M. W.; Johnson, B.; Chen, W.; Wong, M. W.; Gonzalez, C.; Pople, J. A. *Gaussian 03, Revision B.04*; Gaussian, Inc.: Pittsburgh, PA, 2003.

(24) (a) Becke, A. D. *J. Chem. Phys.* **1993**, *98*, 5648−5652. (b) Lee, C.; Yang, W.; Parr, R. G. *Phys. Rev. B* **1988**, *37*, 785−789.

(25) Patersson, G. A.; Al-Laham, M. A. *J. Chem. Phys.* **1991**, *94*, 6081−6090.

(26) Hay, P. J.; Wadt, W. R. *J. Chem. Phys.* **1985**, *82*, 299−310.

(27) (a) Hay, P. J.; Wadt, W. R. *J. Chem. Phys.* **1985**, *82*, 270−283. (b) Wadt, W. R.; Hay, P. J. *J. Chem. Phys.* **1985**, *82*, 284−298.

(28) (a) Stratmann, R. E.; Scuseria, G. E.; Frisch, M. J. *J. Chem. Phys.* **1998**, *109*, 8128−8224. (b) Bauernschmitt, R.; Ahlrichs, R. *Chem. Phys. Lett.* **1996**, *256*, 454−464. (c) Casida, M. E.; Jamorski, C.; Casida, K. C.; Salahub, D. R. *J. Chem. Phys.* **1998**, *108*, 4439−4449.

(29) Frisch, M. J.; Trucks, G. W.; Schlegel, H. B.; Scuseria, G. E.; Robb, M. A.; Cheeseman, J. R.; Scalmani, G.; Barone, V.; Mennucci, B.; Petersson, G. A.; Nakatsuji, H.; Caricato, M.; Li, X.; Hratchian, H. P.; Izmaylov, A. F.; Bloino, J.; Zheng, G.; Sonnenberg, J. L.; Hada, M.; Ehara, M.; Toyota, K.; Fukuda, R.; Hasegawa, J.; Ishida, M.; Nakajima, T.; Honda, Y.; Kitao, O.; Nakai, H.; Vreven, T.; Montgomery, J. A., Jr.; Peralta, J. E.; Ogliaro, F.; Bearpark, M.; Heyd, J. J.; Brothers, E.; Kudin, K. N.; Staroverov, V. N.; Keith, T.; Kobayashi, R.; Normand, J.; Raghavachari, K.; Rendell, A.; Burant, J. C.; Iyengar, S. S.; Tomasi, J.; Cossi, M.; Rega, N.; Millam, J. M.; Klene, M.; Knox, J. E.; Cross, J. B.; Bakken, V.; Adamo, C.; Jaramillo, J.; Gomperts, R.; Stratmann, R. E.; Yazyev, O.; Austin, A. J.; Cammi, R.; Pomelli, C.; Ochterski, J. W.; Martin, R. L.; Morokuma, K.; Zakrzewski, V. G.; Voth, G. A.; Salvador, P.; Dannenberg, J. J.; Dapprich, S.; Daniels, A. D.; Farkas, O.; Foresman, J. B.; Ortiz, J. V.; Cioslowski, J.; Fox, D. J. *Gaussian 09, Revision B.01*; Gaussian, Inc.: Wallingford CT, 2010.

(30) Mandimutsira, B. S.; Chen, S. J.; Reynolds, R. A., III; Coucouvanis, D. *Polyhedron* **1997**, *16*, 3911−3920.

(31) Halbert, T. R.; Pan, W.-H.; Stiefel, E. I. *J. Am. Chem. Soc.* **1983**, *105*, 5476−5477.

(32) Sugimoto, H.; Suyama, K.; Sugimoto, K.; Miyake, H.; Takahashi, I.; Hirota, S.; Itoh, S. *Inorg. Chem* **2008**, *47*, 10150−10157.

(33) Majumdar, A.; Pal, K.; Sarkar, S. *J. Am. Chem. Soc.* **2006**, *128*, 4196−4197.

(34) (a) Maity, R.; Nagarajan, K.; Sarkar, S. *J. Mol. Struct.* **2003**, *656*, 169−176. (b) Nagrajan, K.; Joshi, H. K.; Chaudhury, P. K.; Pal, K.;

Cooney, J. A.; Enemark, J. H.; Sarkar, S. *Inorg. Chem.* **2004**, *43*, 4532−4533.
(35) Das, S. K.; Biswas, D.; Maiti, R.; Sarkar, S. *J. Am. Chem. Soc.* **1996**, *118*, 1387−1397.
(36) Coucouvanis, D.; Hadjikyriacou, A.; Toupadakis, A.; Koo, S. M.; Ilepurama, O.; Draganjac, M.; Salifoglou, A. *Inorg. Chem.* **1991**, *30*, 754−767.
(37) Boyde, S.; Ellis, S. R.; Garner, C. D.; Clegg, W. *J. Chem. Soc., Chem. Commun.* **1986**, 1541−1543.
(38) Draganjac, M.; Simhon, E.; Chan, K. T.; Kanatzidis, M.; Baenziger, N. C.; Coucouvanis, D. *Inorg. Chem.* **1982**, *21*, 3321−3332.
(39) DeHayes, L. J.; Faulkner, H. C.; Doub, W. H., Jr.; Sawyer, D. T. *Inorg. Chem.* **1975**, *14*, 2110−2116.
(40) (a) Majumdar, A.; Pal, K.; Sarkar, S. *Inorg Chem.* **2008**, *47*, 3393−3401. (b) Bose, M.; Moula, G.; Sarkar, S. *Chem. Biodiversity* **2012**, *9*, 1867−1879.
(41) Sproules, S.; Banerjee, P.; Weyhermüller, T.; Yan, Y.; Donahue, J. P.; Wieghardt, K. *Inorg. Chem.* **2011**, *50*, 7106−7122.
(42) Anders, T.; Deeth, R. J.; Nordlander, E. *Inorg. Chem.* **2002**, *41*, 6695−6702.
(43) (a) Kubota, T.; Miyazaki, H. *Bull. Chem. Soc. Jpn.* **1962**, *35*, 1549−1551. (b) Ochaiai, E. *Aromatic Amine Oxides*; Amsterdam: Elsevier, 1967; pp 6−17, 91−97. (c) Simala-Grant, J. L.; Weiner, J. H. *Microbiology* **1996**, *142*, 3231−3239.

dx.doi.org/10.1021/ic4002576 | *Inorg. Chem.* 2013, 52, 5316−5327